TEXTURE MEASUREMENT IN ALUMINUM ALLOY AT HIGH TEMPERATURE

Guizhong Liu, D.K. Rehbein, and R.B. Thompson
Ames Laboratory
Iowa State University
Ames, Iowa 50011

INTRODUCTION

The casting and hot rolling process is a most important and widely used industrial route to produce aluminum alloy sheet[1]. Because rolling is such a high volume process and the capital expenditure in plants and fabrication facilities is so large, even small cost savings or increases in efficiency can result in a very large total money savings[2, 3]. To remove the very costly and time-consuming plant trials, numerical simulation and nondestructive monitoring of the hot rolling process is highly needed.

Studies of mechanical properties and constitutive modeling of a 5182 aluminum alloy under high-temperature deformation by Chen et al [4] show that there are three different deformation mechanism regimes: dynamic strain aging (200°C or below, low strain rate), thermal recovery (200-400°C), and solute drag regime (400°C or higher, low strain rate).

The texture development study by Stout et al[5] shows that the classic (101) deformation texture develops in the dynamic strain aging regime, a combination of (101) deformation texture and (001) cube texture appears in the solute drag regime, and the (001) cube texture occurs at high temperature and high strain rate. Therefore, there are different mechanisms responsible for the texture development during hot rolling deformation.

We presented results of the measurement of the deformation and the static recrystallization texture in aluminum at the 1997 QNDE conference[6]. The present paper is an attempt to trace the texture development at elevated temperature by acoustic NDE technique. The samples were cold rolled and annealed at 372°C, and the transit time was followed during heating, annealing and cooling processes by the specifically designed High-temperature EMAT Inspection System HT-101. Longitudinal wave tests on the samples before and after annealing using conventional piezoelectric transducers were conducted to provide additional information on the texture development. The preliminary results show that the transit time can be tracked during annealing process, and therefore used to monitor the texture development during hot rolling process. However, more research work is needed to make this a fully practical technique.

Review of Progress in Quantitative Nondestructive Evaluation, Vol. 18
Edited by Thompson and Chimenti, Kluwer Academic/Plenum Publishers, 1999

METHODOLOGY

Texture is mathematically described by a quantitative crystallite orientation distribution function using the method of Roe[7]. The crystallite orientation distribution function, $W(\xi, \psi, \phi)$, which expresses the probability of a crystallite having an orientation described by the Euler angles (θ,ψ,ϕ), can be expressed by

$$W(\xi,\psi,\phi) = \sum_{l=0}^{\infty} \sum_{m=-l}^{l} \sum_{n=-l}^{l} W_{lmn} Z_{lmn}(\xi) \exp(-im\psi) \exp(-in\phi) \tag{1}$$

where $\xi=\cos(\theta)$. Here the Z_{lmn} are generalized Legendre functions, and the expansion coefficients, W_{lmn}, are known as orientation distribution coefficients (ODC's).

The ODC's of interest are calculated by

$$W_{400} = \frac{35\sqrt{2}}{64C^o\pi^2}[2\mu - (C_{44} + C_{55})] \tag{2}$$

$$W_{420} = \frac{35\sqrt{2}}{64C^o\pi^2}(C_{55} - C_{44}) \tag{3}$$

$$W_{400} = \frac{35\sqrt{2}}{64C^o\pi^2} \left[C_{33} - (\lambda + 2\mu)\right] \tag{4}$$

where

$$C^o = C_{11}^o - C_{12}^o - 2C_{44}^o \tag{5}$$

$$C_{33} = \rho V_{33}^2 \tag{6}$$

$$C_{55} = \rho V_{13}^2 = \rho V_{31}^2 \tag{7}$$

$$C_{44} = \rho V_{23}^2 = \rho V_{32}^2 \tag{8}$$

where ρ is the density of the material. V_{33} is the longitudinal wave velocity along the normal direction. V_{12} is the shear wave velocity in the rolling direction polarized in the transverse direction. V_{23} is the shear wave velocity in the transverse direction polarized in the normal direction. V_{31} is the shear wave velocity in the normal direction polarized in the rolling direction. Theoretically, $V_{ij} = V_{ji}$ (i, j =1,2,3, which represents rolling, transverse, and normal direction, respectively). λ and μ are the Lame constants of the isotropic aggregate when the crystallites are randomly oriented. C_{11}^o, C_{12}^o, and C_{44}^o are the elastic constants of the single crystal.

The velocity can be calculated by

$$V = \frac{s}{t} \tag{9}$$

where s is the thickness of the sample which is related to the thickness s_0 of the sample at room temperature (T_o) by

$$s = s_o(1 + \alpha\, \Delta T) \tag{10}$$

where α is the linear thermal expansion coefficient of the sample. ΔT is the temperature rise. t is the transit time (or time-of-flight) which can be measured by the phase-slope technique.

EXPERIMENTAL SETUP

Figure 1 below shows the schematic diagram of the experimental setup. The EMAT transducer is excited by a tone-burst signal generated by a Ritec RAM-10000 system, which also receives and amplifies the transmitted signals for processing. The received signal is monitored by the LeCroy 9400 oscilloscope. The circulated cooling water keeps the transducer from being heated to high temperature. The temperature of the water bath providing the circulating water was manually controlled between 24-26°C. The furnace temperature is controlled and recorded.

A bar of the testing material was cut from the aluminum plate (the detail of the material can be found in [6]) and cold rolled to 39.6% thickness reduction. Then, the samples were cut and machined to the size about 51×51×12 mm. Two samples were tested, one with ultrasound wave polarized parallel to RD and another with the polarization parallel to TD direction. In each case the wave propagated along ND direction.

The temperature of the sample was calibrated against the furnace temperature, using a dummy sample under the same experimental conditions.

The phase of one echo is a linear function of frequency. The slope of this linear function contains time information. The transit time for the sound to travel through one thickness of the sample is determined by the following equation:

$$Transit \quad time = \frac{\left(\frac{\Delta\phi_{r2}}{\Delta F} - \frac{\Delta\phi_{r1}}{\Delta F}\right)}{4\pi(N_2 - N_1)} \tag{11}$$

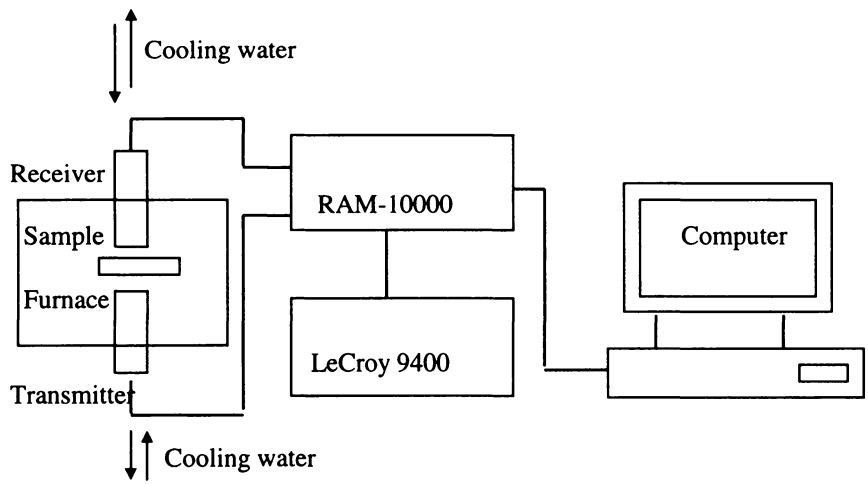

Figure 1. A schematic showing the experimental setup.

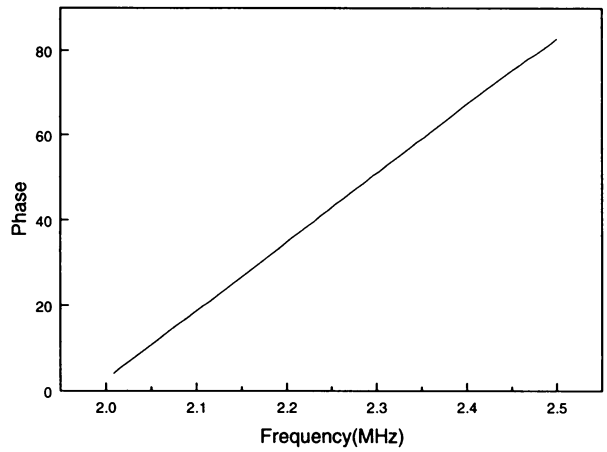

Figure 2 A typical phase difference versus frequency curve.

where N_2 is the echo number of the later echo and N_1 is the number of the earlier one. ΔF is the frequency interval correspondent to the phase interval $\Delta\phi_{r1}$ for the earlier echo, $\Delta\phi_{r2}$ for the later echo.

The phase difference for the two measuring echoes as a function of frequency is shown in the following Figure 2. The slope of this curve is used to determine the transit time.

RESULTS AND DISCUSSIONS

Figure 3 below plots the transit time and the furnace temperature versus the testing time during the whole heating, annealing and cooling process. During heating, the transit time increases as the temperature increases because of the thermal expansion and the

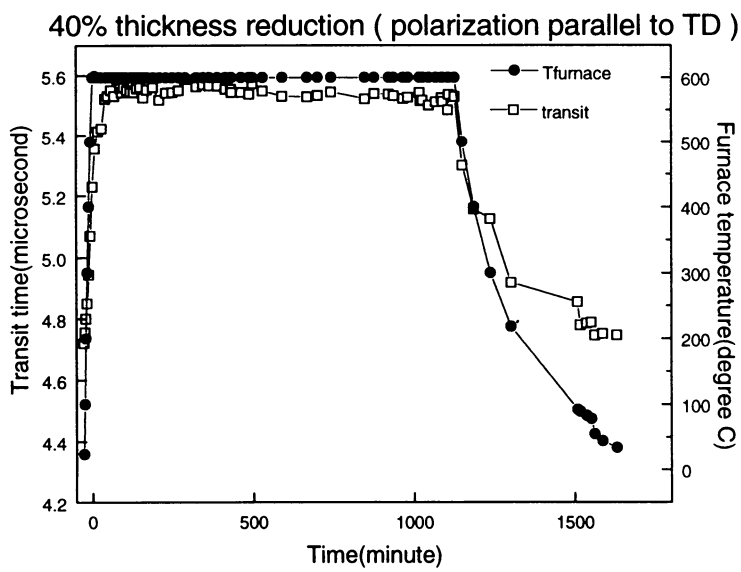

Figure 3 Transit time and furnace temperature versus time.

decrease in elastic constant. After the furnace reaches the set temperature (600° C), the transit time increases with decreasing rate because it takes about 30 minutes for the system to reach the equilibrium state. At high temperature, after a holding time of about 10 hours, the transit time starts to decrease, or the shear wave velocity increases. The recrystallization process might be responsible for this transit time decreasing with more evidence needed. During the cooling process, the transit time decreases.

The transit time cycle as a function of temperature during the whole testing process is shown in Figure 4. The transit time after cooling is different from the starting point transit time, which is expected because of the recrystallization process undergone during the annealing stage. However, the two samples have different trend: the sample tested with wave polarization parallel to TD has longer transit time than the starting point value, while the sample with wave polarization parallel to RD has shorter transit time than its starting point value. The values are listed in Table 1 below, where measurements in TA1 sample were polarized parallel to RD, and those in TA2 were polarized parallel to TD; the shear and longitudinal velocities and the attenuation at 20 MHz are also listed for each sample before and after annealing.

Based on the data listed in Table1 above, the ODC's can be calculated by using Equations 3-9 and the materials constants listed in[6]. The results are shown in Table 2. W_{400} and W_{420} are calculated by the shear wave velocity measurement result, while W_{400}^{L} is calculated from the longitudinal wave velocity measurement. The positive values of W_{400} before annealing indicate the presence of the cube recrystallization texture, which is

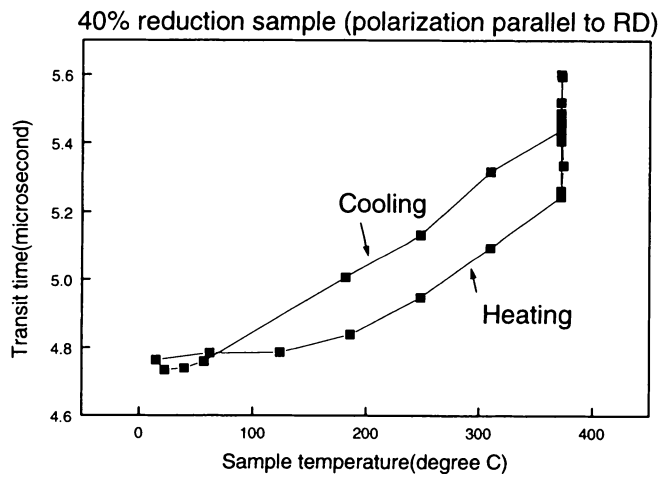

Figure 4 transit time cycle during testing process.

Table 1 40% reduction Al sample.

Sample	TA1		TA2	
Annealing	Before	After	Before	After
V^T (m/s)	3164.8	3184.5	3194.8	3177.3
V^L (m/s)	6356.83	6380.11	6356.37	6384.34
α (Np/cm)	0.052	0.014	0.054	0.023

Table 2 ODC's before and after annealing (40% reduction Al sample), $\times 10^{-3}$.

Sample	TA1		TA2	
Annealing	Before	After	Before	After
W_{400}	0.8	1.1		
W_{420}	2.5	-0.9		
W_{400}^{L}	9.5	3.8	9.6	2.7

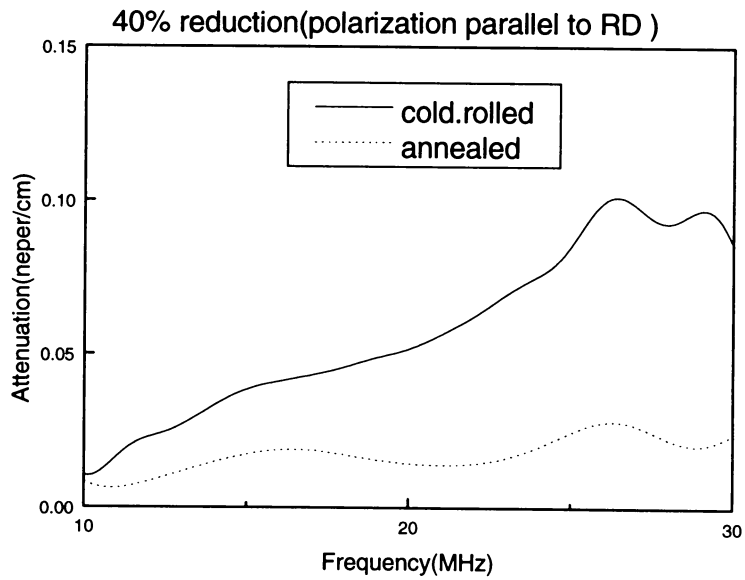

Figure 5 Attenuation measurement results.

consistent with our previous results[6] which showed that the deformation texture dominates only beyond 50% thickness reduction. After annealing, the negative value of W_{420} indicates that other texture components besides cube texture exist in the sample. Whether it proves the results of Stout[5] or not, we do not know for the time being. We are unable at this time to explain why W_{400} calculated from shear wave and longitudinal wave measurements shows a different trend before and after annealing. The possible reasons might include materials constants chosen, the error bars in the transit time and/or thickness measurement, and the microstructure change during recrystallization which will change the elastic constant, etc.

The ultrasonic attenuation measurement results are shown in Figure 5 above. The solid line shows the attenuation of the sample before annealing, and the dotted line represents the attenuation of the sample after annealing. The attenuation decrease is consistent with the fact that the recrystallization produces smaller grain size.

SUMMARY REMARKS

The preliminary tests on the High Temperature EMAT Inspection System HT 101 yield promising results of the shear velocity, which can be used to track the texture development at high temperature. The starting texture of the materials tested has a weak cube component even after 40% thickness reduction. The annealing texture has cube and

other components co-existing in the sample. The room temperature analysis of texture and attenuation is consistent with our previous results[6].

However, we have some difficulties to explain all our data obtained so far. The problems we encountered during experiments include the temperature difference between the sample and the transducers, and the temperature gradient in the sample. Temperature effects on the transit time are not clear so far. Besides, it takes about 40 seconds to obtain the transit time information. More experience is needed to run this system in order to obtain tractable data.

More samples with different cold rolling extents are being prepared. Longitudinal wave EMAT transducers have been ordered in order to obtain W_{440}.

ACKNOWLEDGMENT

Ames Laboratory is operated for the US Department of Energy by Iowa State University under Contract W-7405-ENG-82. This work was supported by the Office of Basic Energy Sciences as a part of the Center of Excellence of the Synthesis and Processing of Advanced Materials.

REFERENCES

1. H.E. Ekstrom and P. Charlier, in Aluminum Alloys for Packaging II, ed. J.G. Morris, S.K. Das and H.S. Goodrich, A Publication of The Minerals, Metals & Materials Society, Warrendale, Pennsylvania, 1996, pp. 245-251.
2. S.M. Knap, in Aluminum Alloys for Packaging II, ed. J.G. Morris, S.K. Das and H.S. Goodrich, A Publication of The Minerals, Metals & Materials Society, Warrendale, Pennsylvania, 1996, pp. 97-106.
3. F.J. Humphreys and M. Hatherly, Recrystallization and Related Annealing Phenomena, Pergamon Press, 1995.
4. S.R. Chen, M.G. Stout, U.F. Kocks, S.R. MacEwen and A.J. Beaudoin, "Constitutive Modeling of a 5182 Aluminum as a Function of Strain Rate and Temperature", to be presented and published in Hot Deformation of Aluminum Alloys II Symposium, Ed. T.R. Bieler, L. Lalli, and S.R. MacEwen, 1998 TMS Fall Meeting, Rosemont, Illiois.
5. M.G. Stout, S.R. Chen, U.F. Kocks, A.J. Schwartz, S.R. MacEwen and A.J. Beaudoin, "Mechanisms Responsible for Texture Development in a 5182 Aluminum Alloy Deformed at Elevated Temperature", to be presented and published in Hot Deformation of Aluminum Alloys II Symposium, Ed. T.R. Bieler, L. Lalli, and S.R. MacEwen, 1998 TMS Fall Meeting, Rosemont, Illiois.
6. G. Liu, F. Laabs, D. Rehbein, O. Buck, and R.B. Thompson, QNDE, 1998, Vol. 17B, pp. 1899-1906.
7. R.J. Roe, J. Appl. Phys., 1965, Vol.36, p2024.